NANO LETTERS

pubs.acs.org/NanoLett

Synthesis of Few-Layer Hexagonal Boron Nitride Thin Film by Chemical Vapor Deposition

Yumeng Shi,[†,‡] Christoph Hamsen,[†,§] Xiaoting Jia,[∥] Ki Kang Kim,[†] Alfonso Reina,[∥] Mario Hofmann,[†] Allen Long Hsu,[†] Kai Zhang,[†] Henan Li,[‡] Zhen-Yu Juang,[#] Mildred. S. Dresselhaus,[†,⊥] Lain-Jong Li,[*,#] and Jing Kong[*,†]

[†]Department of Electrical Engineering and Computer Sciences, Massachusetts Institute of Technology, Cambridge, Massachusetts 02139, [‡]School of Materials Science and Engineering, Nanyang Technological University, 50 Nanyang Avenue, Singapore 639798, Singapore, [§]Department of Physics, Technische Universität München, Arcisstrasse 21, München 80333, Germany, [∥]Department of Materials Science and Engineering, Massachusetts Institute of Technology, Cambridge, Massachusetts 02139, [⊥]Department of Physics, Massachusetts Institute of Technology, Cambridge, Massachusetts 02139, and [#]Research Center for Applied Science, Academia Sinica, Taipei 11529, Taiwan

ABSTRACT In this contribution we demonstrate a method of synthesizing a hexagonal boron nitride (*h*-BN) thin film by ambient pressure chemical vapor deposition on polycrystalline Ni films. Depending on the growth conditions, the thickness of the obtained *h*-BN film is between ~5 and 50 nm. The *h*-BN grows continuously on the entire Ni surface and the region with uniform thickness can be up to 20 μm in lateral size which is only limited by the size of the Ni single crystal grains. The hexagonal structure was confirmed by both electron and X-ray diffraction. X-ray photoelectron spectroscopy shows the B/N atomic ratio to be 1:1.12. A large optical band gap (5.92 eV) was obtained from the photoabsorption spectra which suggest the potential usage of this *h*-BN film in optoelectronic devices.

KEYWORDS Hexagonal boron nitride, chemical vapor deposition, borazine

Boron nitride (BN) is isoelectronic to the similarly structured carbon lattice while consisting of an equal number of boron and nitrogen atoms. Like carbon materials, it has been found that BN exists in various crystalline structures, such as amorphous (*a*-BN), hexagonal (*h*-BN), cubic (*c*-BN), and wurtzite (*w*-BN) lattices. Analogous to graphite, within each *h*-BN layer, boron and nitrogen atoms are bound together by strong covalent bonds, forming a *h*-BN sheet, while between the different layers a weak van der Waals force occurs. Boron nitride films have a wide range of attractive properties, including high temperature stability, a low dielectric constant, high mechanical strength, a large thermal conductivity, high hardness, and high corrosion resistance, leading to a number of potential applications as both a structural and electronic material.[1−5] Furthermore, *h*-BN powder is traditionally used as a lubricant. Due to its good electrical insulation properties, *h*-BN has also been applied as a charge leakage barrier layer for electronic equipment. Recently, far-ultraviolet (FUV) light-emitting devices based on *h*-BN have been demonstrated to be an alternative way for implementing compact UV optoelectronics.[5] Nevertheless, due to the challenges in synthesizing high-quality *h*-BN, the materials properties of *h*-BN have not yet been well understood. For example, it was previously suggested that *h*-BN is an indirect-band-gap semiconductor,[6,7] whereas more recent studies have shown that *h*-BN exhibits a direct band gap of 5.9 eV.[8] This discrepancy is most likely due to the previous lack of high-quality *h*-BN films. Only with the single crystal *h*-BN flakes made by Watanabe et al.[8] have the direct band gap properties been observed and evidence for UV lasing been provided. The availability of high-quality *h*-BN flakes also opened up the application of *h*-BN in far-ultraviolet (FUV) light-emitting diodes (LEDs).[4,5] In addition to the optoelectronic applications, *h*-BN also shows great potential in high-performance electronic devices. In recent years, graphene, one monolayer of graphite, has been considered to be an ideal material for the fabrication of nanoelectronic devices due to its excellent electrical properties. It was suggested that due to the close match of the lattice parameters between *h*-BN and graphene, epitaxial graphene on *h*-BN would give rise to a band gap opening of graphene,[9] and potentially *h*-BN can also serve as a good gate dielectric for graphene transistors. Therefore, having high-quality *h*-BN for epitaxial deposition of graphene is highly desirable. Monolayer and few-layer *h*-BN flakes can be exfoliated from bulk BN crystals by either mechanical cleavage[10] or a chemical-solution-derived method.[11,12] How-

* To whom correspondence should be addressed, (J.K.) jingkong@mit.edu and (L.-J.L.) lanceli@gate.sinica.edu.tw.

Received for review: 07/7/2010
Published on Web: 09/02/2010

DOI: 10.1021/nl1023707 | *Nano Lett.* **2010,** *10,* 4134–4139

ever, the flake size is usually limited which could hinder the further application of *h*-BN in this way. Compared to the top-down method, chemical routes offer significant advantages for obtaining large area *h*-BN films. Current methods for obtaining *h*-BN thin films by chemical vapor deposition (CVD) include the use of various chemical precursors such as BF_3/NH_3,[13] BCl_3/NH_3,[14] B_2H_6/NH_3.[15] For these systems, controlling the ratio between the boron source and NH_3 is critical for obtaining stoichiometric *h*-BN layers. Furthermore, the deposition rate is also affected by the molar ratio of the boron source and NH_3. Synthesizing a *h*-BN thin film via the pyrolysis of a single precursor such as borazine ($B_3N_3H_6$),[16] trichloroborazine ($B_3N_3H_3Cl_3$),[17,18] or hexachloroborazine ($B_3N_3Cl_6$)[19] shows many advantages due to the 1:1 B/N stoichiometry. A further benefit of borazine is that it does not exhibit the high toxicity of other boron containing precursors such as BF_3 or BCl_3. Previously it was also demonstrated that well-ordered monolayers of *h*-BN can be obtained by exposing borazine to Ni(111)[20] or other transition metal surfaces[21,22] at high temperatures (>700 °C). However, this method requires expensive ultrahigh vacuum (UHV) chambers. In addition, the *h*-BN growth under UHV conditions appears to be self-limiting to one monolayer, and the growth of multilayers turns out to be difficult.[20,22] For large scale electronics applications, it is necessary to obtain large area, high-quality, well-ordered layer structured *h*-BN thin films, ideally with a controlled thickness. In this work, we demonstrate the synthesis of large area *h*-BN thin films with atomically smooth surface morphology on polycrystalline Ni by using a low-cost ambient pressure chemical vapor deposition (APCVD) system. The growth temperature can be reduced to 400 °C, which is followed by a postannealing process at 1000 °C yielding a high-quality *h*-BN thin film. The thickness of the film is not limited to a monolayer, and at present it is in the range of 5−50 nm. Furthermore, the as-grown *h*-BN thin film can be transferred to arbitrary substrates by releasing it from the underlying Ni layer. The transfer capability opens the way for further characterizations of the *h*-BN thin film and for many potential applications.

Results and Discussion. The *h*-BN thin film was obtained in an APCVD system, by exposure of polycrystalline Ni to borazine ($B_3N_3H_6$) vapor carried by N_2 gas flow (see Supporting Information). The growth temperature was adjusted from 700 °C down to 400 °C. Thermal decomposition of borazine at a high temperature (>700 °C) on transition metal surfaces under vacuum conditions usually leads to a self-limiting growth, which forms monolayer *h*-BN.[23−26] However, it is reported that the dehydrogenation reaction of borazine on metal surfaces occurs over a very broad temperature range.[27] According to the thermogravimetric analysis for the ceramic conversion reaction of borazine, it is found that borazine is converted to polyborazylene at ∼70 °C, and the resulting polymer then undergoes a two-stage weight loss and eventually forms elementally pure boron nitride:[28,29] the weight loss of polyborazylene is initiated from 125 to 300 °C, which is due to the two-dimensional cross-linking reaction of B−H and N−H groups on adjacent chains; the second weight loss continues from 700 °C up to 1100 °C, which is suggested to be due to the hydrogen loss from the unaligned chain branches of polyborazylene and ultimately forming *h*-BN.[29,30] Therefore, in order to synthesize a few layer *h*-BN thin film with high quality, a moderate temperature (400 °C) is chosen. At this temperature, a polymerization reaction takes place and forms polyborazylene which could further be dehydrogenated to form *h*-BN. We noticed that by further increasing the growth temperature, either a rough surface morphology is formed or *h*-BN particles (see Figure S1 in Supporting Information) rather than continuous films occur, which could be due to the fast decomposition rate of polyborazylene at high temperature and/or the poor wetting between the precursor and the Ni surface. Therefore a postannealing procedure was used after the exposure of the Ni to borazine: the temperature was gradually increased from 400 to 1000 °C at a rate of 5 °C/min and was maintained at 1000 °C for 1 h. This postannealing process facilitates the further dehydrogenation of borazine and also results in a better crystallinity of the *h*-BN. After the sample was cooled down to room temperature, a transparent thin film can be observed on the Ni surface. The thickness of the *h*-BN grown upon exposure of 1 sccm borazine for 30 min is around 5 nm. Thicker films up to 50 nm can be grown by increasing the flow rate of borazine to 10 sccm for 1 h. A more detailed study on the thickness dependence of the *h*-BN synthesis process is underway.

By wet-etching of the underlying Ni film, the CVD-derived thin *h*-BN film can be transferred to arbitrary substrates,[31] which greatly extends the potential application of the *h*-BN film (see Supporting Information). Optical images of the as-grown *h*-BN films on Ni and of the *h*-BN films transferred to SiO_2/Si substrates are shown in Figure 1A and Figure 1B, respectively. The images show that the *h*-BN film covers the whole area defined by the nickel film. The film thickness is homogeneous on top of each Ni grain, whereas along the Ni grain boundaries the *h*-BN layer is noticeably thicker. The surface morphology of the *h*-BN was further characterized by atomic force microscopy (AFM). Figure 1C and Figure 1D show the AFM image of the as-grown *h*-BN film on a Ni surface and the one that was transferred to a SiO_2/Si substrate, respectively. The AFM images indicate that the *h*-BN films tend to follow the morphology of the Ni surface after growth (Figure 1C).

Transmission electron microscopy (TEM) with a JEOL 2010F was used to characterize the structure of the *h*-BN thin films, and the results are shown in Figure 2. The CVD grown *h*-BN films were transferred to Quantifoil holey carbon grids, as is shown by the low magnification TEM image in Figure 2A. The film tends to form wrinkles in the center of the grids, making it easier to distinguish the presence of the thin film. In Figure 2B an electron diffraction pattern was taken on the smooth region of the film to reveal the hexagonal lattice

DOI: 10.1021/nl1023707 | *Nano Lett.* **2010,** *10,* 4134–4139

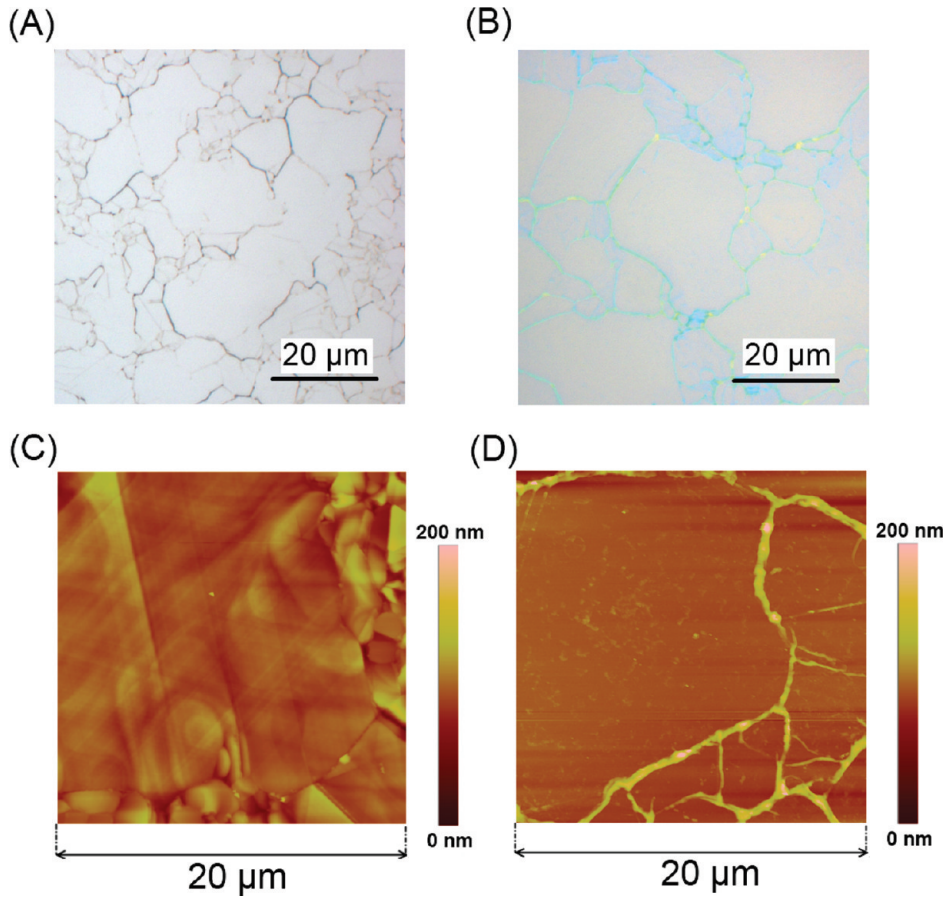

FIGURE 1. Morphology of a *h*-BN thin film: (A) optical image of a *h*-BN thin film on a Ni substrate; (B) optical image of a *h*-BN thin film transferred onto a SiO_2/Si substrate; (C) AFM image of a *h*-BN thin film on a Ni Substrate; (D) AFM image of a *h*-BN thin film on a SiO_2/Si substrate.

structure of the material. The electron beam size is ~50 nm, and the in plane lattice constant can be estimated to be around 0.25 ± 0.03 nm from the electron diffraction pattern which is in good agreement with earlier published values of 0.25 nm.[32,33] Sometimes different diffraction patterns with a set of secondary diffraction spots can be observed, presumably due to the presence of wrinkles or the folding of layers. In some regions the film is broken and the edges are suspended across the TEM grid openings. Figure 2C shows the TEM image of an edge region. Similar to observations on graphene sheets,[34] the edges of a suspended *h*-BN film also tend to fold back,[35,36] allowing for a cross sectional view of the film. In Figure 2D parallel line features can be observed along the edge of the film under high magnification, similar to the case of graphene films. This allows not only the counting of the number of layers of the film but also measurement of the interlayer distance as well, which is around 0.35 ± 0.02 nm, consistent with the reported value for the *h*-BN structure.[35] Figure 2E shows a high-resolution TEM image taken from the *h*-BN surface. These TEM characterizations of the *h*-BN film reveal the single crystal nature of the examined areas, indicating the high quality of the synthesized *h*-BN thin films.

The hexagonal crystal structure was further confirmed by X-ray diffraction measurements (XRD) of the *h*-BN thin film with a thickness of ~50 nm on a SiO_2/Si substrate, as shown in Figure 3. The *h*-BN (0002) peak at around 26.7° can be identified (see Figure S2 in the Supporting Information). The estimation of the interlayer spacing according to Bragg's law is 0.33 nm, which is consistent with the value from the TEM measurement. The peak around 34° is due to the Si⟨100⟩ substrate as directly verified in our experiment. The broad diffraction peak from 20° to 35° could originate from semicrystalline BN, which has an elongated lattice constant *c*.[37]

X-ray photoelectron spectroscopy (XPS) was also applied to characterize the elemental stoichiometry of the synthesized *h*-BN samples. Figure 4 shows the XPS spectra of the as-grown *h*-BN thin film on a Ni substrate with a film thickness of ~5 nm. The binding energies for nitrogen 1s and boron 1s are shown in parts A and B of Figure 4, respectively. The observed binding energies of N 1s and B 1s from the XPS measurement are 398.2 and 190.75 eV, respectively. The values are in good agreement with the literature values.[38,39] The B/N ratio from our XPS survey was calculated to be 1.12. The additional oxygen and carbon

DOI: 10.1021/nl1023707 | *Nano Lett.* **2010,** *10,* 4134–4139

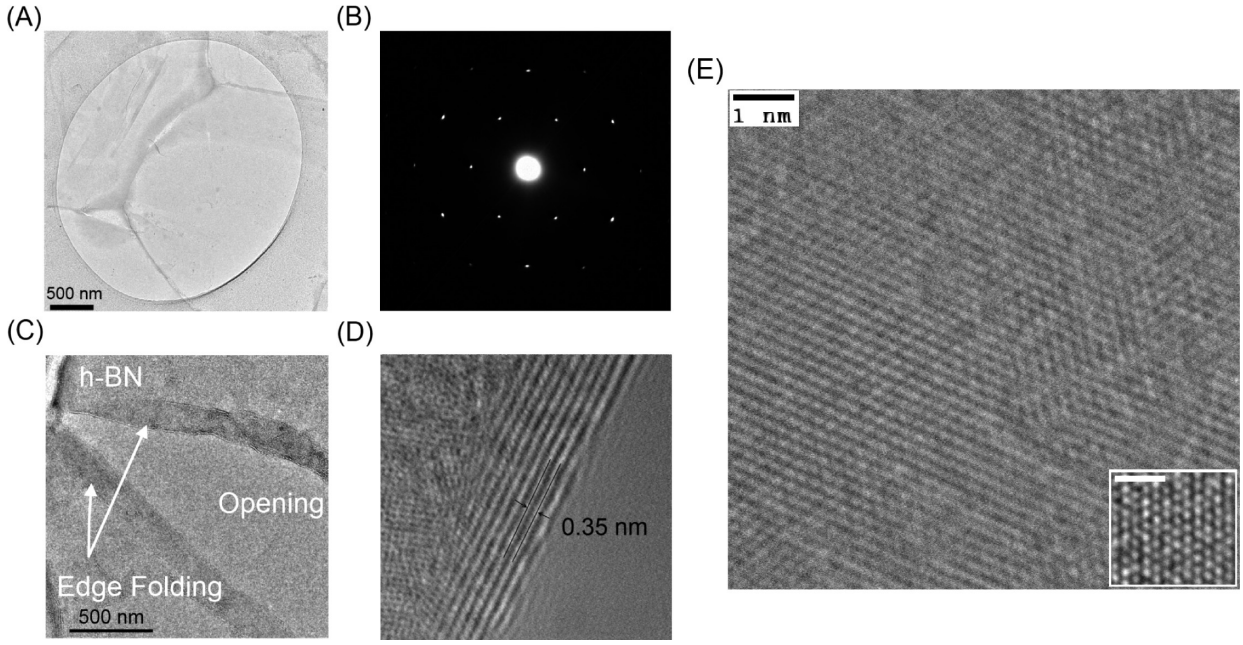

FIGURE 2. TEM images of a *h*-BN thin film: (A) low-magnification TEM image showing a CVD-grown *h*-BN thin film on a Quantifoil holey carbon grid; (B) electron diffraction pattern of the *h*-BN thin film taken from a freely suspended region; (C−E) TEM images of the *h*-BN thin film under different magnifications. (C) TEM image showing a broken part of the *h*-BN thin film and the edge folding. High-magnification TEM image showing the edges (D) and the surface region (E) of the film, with the inset of figure (E) showing a close-up high resolution TEM image on the *h*-BN surface, and the scale bar is 1 nm.

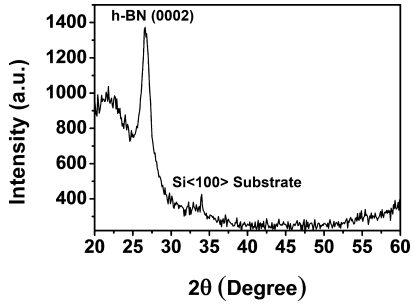

FIGURE 3. Crystal structure characterization. XRD characterization of a *h*-BN thin film on a SiO_2/Si substrate.

peaks shown in Figure 4C could result from the exposure of the *h*-BN film to air in between the film growth and the XPS measurement. The small nickel 3s and 3p peaks could be from the underlying substrate since the X-ray is expected to penetrate through the *h*-BN film down to 3−5 nm.

Raman and Fourier transform infrared (FTIR) spectroscopy are useful techniques to analyze the *h*-BN lattice vibration modes which are due to the stretching of the bonds between the nitrogen and boron atoms. Figure 5 shows the Raman and FTIR spectra from a *h*-BN film with a thickness of ∼50 nm. Thicker films were chosen in order to obtain a stronger signal. Figure 5A shows the FTIR spectra of both the synthesized *h*-BN films and the bare Si substrate. The strong absorption band centered at 1369.5 cm^{-1} is assigned to the in-plane ring vibration (E_{1u} mode) of the *h*-BN sample.[40] The vibration peak centered around 822.8 cm^{-1} (A_{2u} mode) is characteristic for the out-of-plane *h*-BN vibration.[40] All the other peaks in the FTIR spectra can be attributed to the underlying Si substrate. For the Raman measurement, the films were transferred to SiO_2/Si substrates and the excitation wavelength used for the Raman measurement was 532 nm. The Raman spectrum in Figure 5B shows one dominant peak at 1367.8 cm^{-1} which can be assigned to the E_{2g} vibration mode of *h*-BN.

The good quality of the CVD *h*-BN films makes them an excellent candidate for both optoelectronic and electronic applications. To investigate the optical properties, UV−visible absorption spectra of the *h*-BN thin film were taken and the results are shown in Figure 6A. According to the equation $A = \alpha l$, where A is the optical absorption of the thin film obtained from the measurement and l is the thickness of the film, we can estimate the absorption coefficient α at various photon energies (E), if the thickness of the film is known. Furthermore, the optical band gap (OBG) can be obtained by considering a direct transition between the valence and conduction bands. For direct gap semiconductors such as *h*-BN, the absorption coefficient is given as $\alpha = C(E - E_g)^{1/2}/E$.[41] Here, C is a constant and E_g is the OBG energy. Therefore, for an allowed direct transition, the power law behavior of $(\alpha E)^2 \propto (E - E_g)$ can be derived from the aforementioned equation. The plot of $(\alpha E)^2$ vs E should give a straight line, and when $(\alpha E)^2 = 0$ the corresponding E value should be equal to E_g. Using this method, the OBG of *h*-BN film can be extracted as shown in Figure 6B. For an *h*-BN film with a thickness of 5 nm, the E_g is estimated from Figure 6B

DOI: 10.1021/nl1023707 | *Nano Lett.* **2010,** *10,* 4134–4139

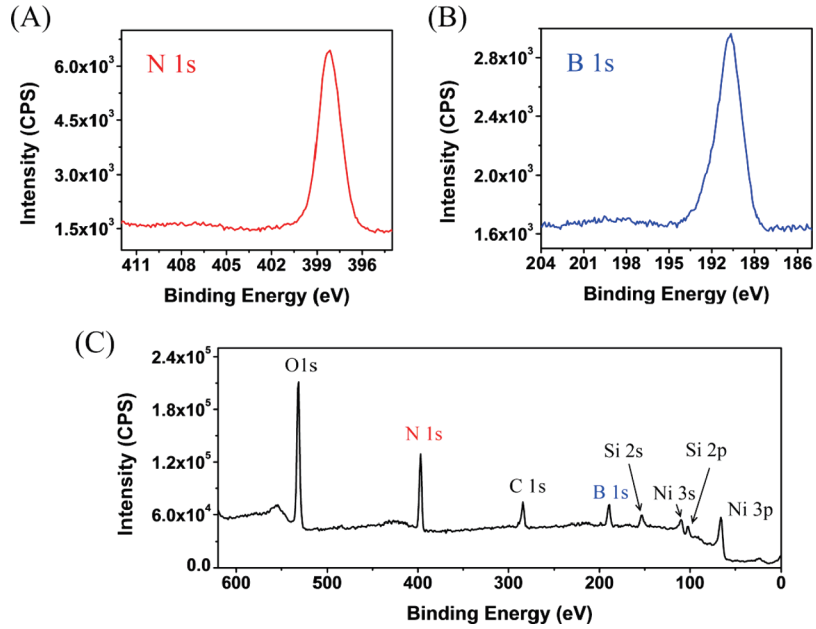

FIGURE 4. Boron and nitrogen atomic ratio analysis: (A) N 1s and (B) B 1s XPS spectra shown, respectively, of a *h*-BN film; (C) XPS survey of the *h*-BN thin film on a Ni/SiO_2/Si substrate.

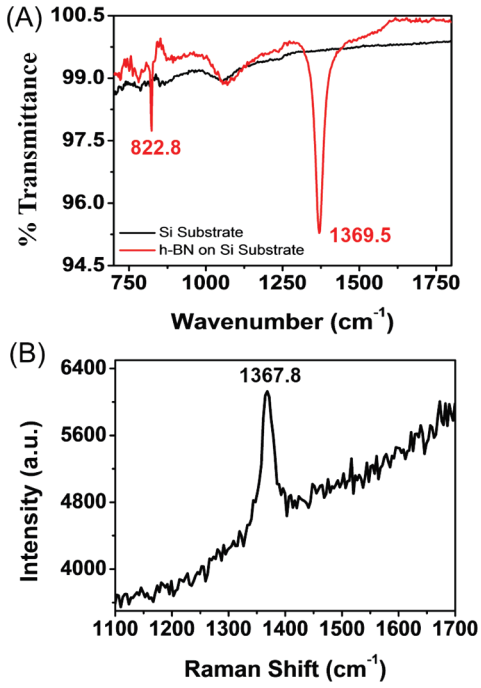

FIGURE 5. FTIR and Raman spectroscopy: (A) FTIR spectra of a bare Si substrate and a *h*-BN thin film on a Si substrate; (B) Raman spectra of a *h*-BN thin film on a SiO_2/Si substrate.

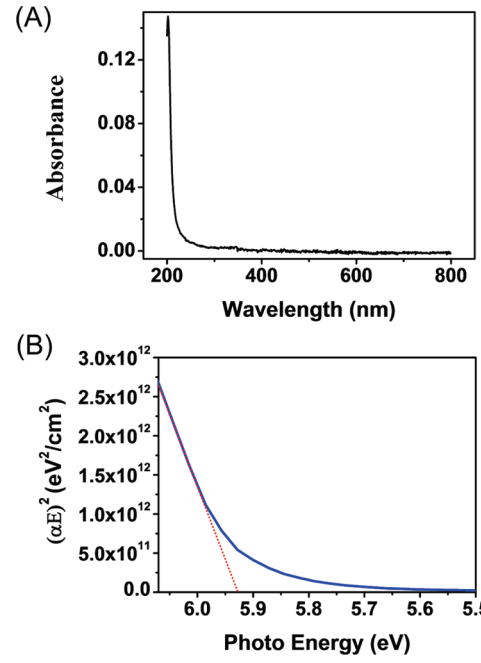

FIGURE 6. UV−visible absorption spectra and optical band gap analysis: (A) optical absorption spectrum of a *h*-BN thin film transferred onto a quartz substrate; (B) optical band gap analysis from (A).

to be around 5.92 eV which is consistent with the observations by Watanabe et. al[6] (5.9 eV). Further characterizations which can provide direct evidence of the OBG such as cathodoluminescence would be desirable to confirm this result.

In summary, large area (~cm^2) *h*-BN thin films on nonspecific substrates can be obtained by CVD synthesis using a Ni substrate followed by a film transfer technique. The thicknesses of these *h*-BN films are in the range of a few to tens of nanometers. Initial characterizations have confirmed the crystalline nature of the films with a B/N ratio close to the stoichiometric B/N ratio. A band gap energy of 5.92 eV can be derived from the optical absorption data. With these *h*-BN films many interesting investigations can be envisioned which will lead to important

DOI: 10.1021/nl1023707 | *Nano Lett.* **2010,** *10,* 4134–4139

applications such as UV light emitting thin films for optoelectronic applications and the dielectric layers for graphene electronic applications.

Acknowledgment. This work is partially supported by the National Science Foundation under award number NSF DMR 0845358. Y. Shi and L. J. Li acknowledge the support by the nano program at Academia Sinica, National Science Council Taiwan (NSC-99-2112-M-001-021-MY3) and support from the National Research Foundation in Singapore (NRF-CRP-07-2). M. Hofmann, J. Kong, and M. S. Dresselhaus acknowledge support from the Graphene Approaches to Terahertz Electronics (GATE)—MURI Grant N00014-09-1-1063.

Supporting Information Available. AFM image of the *h*-BN film on Ni sample obtained by flashing 1 sccm borazine vapor under 900 °C, XRD peak fitting and film thickness estimation using the Scherrer equation, and a detailed description of the fabrication methods. This material is available free of charge via the Internet at http://pubs.acs.org.

REFERENCES AND NOTES

(1) Kho, J.-G.; Moon, K.-T.; Kim, J.-H.; Kim, D.-P. *J. Am. Ceram. Soc.* **2000**, *83* (11), 2681–2683.
(2) Sugino, T.; Tai, T. *Jpn. J. Appl. Phys., Part 2* **2000**, *39* (11A), L1101–L1104.
(3) Haubner, R.; Wilhelm, M.; Weissenbacher, R.; Lux, B. *Struct. Bonding (Berlin)* **2002**, *102*, 1–45.
(4) Kubota, Y.; Watanabe, K.; Tsuda, O.; Taniguchi, T. *Science* **2007**, *317* (5840), 932–934.
(5) Watanabe, K.; Taniguchi, T.; Niiyama, T.; Miya, K.; Taniguchi, M. *Nat. Photonics* **2009**, *3* (10), 591–594.
(6) Catellani, A.; Posternak, M.; Baldereschi, A.; Freeman, A. J. *Phys. Rev. B* **1987**, *36* (11), 6105.
(7) Solozhenko, V. L.; Lazarenko, A. G.; Petitet, J. P.; Kanaev, A. V. *J. Phys. Chem. Solids* **2001**, *62* (7), 1331–1334.
(8) Watanabe, K.; Taniguchi, T.; Kanda, H. *Nat. Mater.* **2004**, *3* (6), 404–409.
(9) Giovannetti, G.; Khomyakov, P. A.; Brocks, G.; Kelly, P. J.; van den Brink, J. *Phys. Rev. B* **2007**, *76*, No. 073103.
(10) Pacile, D.; Meyer, J. C.; Girit, C. O.; Zettl, A. *Appl. Phys. Lett.* **2008**, *92* (13), 133107–3.
(11) Han, W.-Q.; Wu, L.; Zhu, Y.; Watanabe, K.; Taniguchi, T. *Appl. Phys. Lett.* **2008**, *93* (22), 223103–3.
(12) Zhi, C.; Bando, Y.; Tang, C.; Kuwahara, H.; Golberg, D. *Adv. Mater.* **2009**, *21* (28), 2889–2893.
(13) Pierson, H. O. *J. Compos. Mater.* **1975**, *9* (3), 228–240.
(14) Rozenberg, A. S.; Sinenko, Y. A.; Chukanov, N. V. *J. Mater. Sci.* **1993**, *28* (20), 5528–5533.
(15) Middleman, S. *Mater. Sci. Eng., A* **1993**, *163* (1), 135–140.
(16) Adams, A. C. *J. Electrochem. Soc.* **1981**, *128* (6), 1378–1379.
(17) Auwarter, W.; Suter, H. U.; Sachdev, H.; Greber, T. *Chem. Mater.* **2004**, *16* (2), 343–345.
(18) Muller, F.; Stowe, K.; Sachdev, H. *Chem. Mater.* **2005**, *17* (13), 3464–3467.
(19) Constant, G.; Feurer, R. *J. Less-Common Met.* **1981**, *82* (1−2), 113–118.
(20) Nagashima, A.; Tejima, N.; Gamou, Y.; Kawai, T.; Oshima, C. *Phys. Rev. B* **1995**, *51* (7), 4606–4613.
(21) Nagashima, A.; Tejima, N.; Gamou, Y.; Kawai, T.; Oshima, C. *Surf. Sci.* **1996**, *357* (1−3), 307–311.
(22) Corso, M.; Auwarter, W.; Muntwiler, M.; Tamai, A.; Greber, T.; Osterwalder, J. *Science* **2004**, *303* (5655), 217–220.
(23) Morscher, M.; Corso, M.; Greber, T.; Osterwalder, J. *Surf. Sci.* **2006**, *600* (16), 3280–3284.
(24) Nagashima, A.; Tejima, N.; Gamou, Y.; Kawai, T.; Oshima, C. *Phys. Rev. Lett.* **1995**, *75* (21), 3918–3921.
(25) Preobrajenski, A. B.; Vinogradov, A. S.; Martensson, N. *Surf. Sci.* **2005**, *582* (1−3), 21–30.
(26) Auwarter, W.; Muntwiler, M.; Osterwalder, J.; Greber, T. *Surf. Sci.* **2003**, *545* (1−2), L735–L740.
(27) Paffett, M. T.; Simonson, R. J.; Papin, P.; Paine, R. T. *Surf. Sci.* **1990**, *232* (3), 286–296.
(28) Fazen, P. J.; Beck, J. S.; Lynch, A. T.; Remsen, E. E.; Sneddon, L. G. *Chem. Mater.* **1990**, *2* (2), 96–97.
(29) Fazen, P. J.; Remsen, E. E.; Beck, J. S.; Carroll, P. J.; McGhie, A. R.; Sneddon, L. G. *Chem. Mater.* **1995**, *7* (10), 1942–1956.
(30) Chan, V. Z. H.; Rothman, J. B.; Palladino, P.; Sneddon, L. G.; Composto, R. J. *J. Mater. Res.* **1996**, *11* (2), 373–380.
(31) Reina, A.; Son, H. B.; Jiao, L. Y.; Fan, B.; Dresselhaus, M. S.; Liu, Z. F.; Kong, J. *J. Phys. Chem. C* **2008**, *112* (46), 17741–17744.
(32) Auwärter, W.; Kreutz, T. J.; Greber, T.; Osterwalder, J. *Surf. Sci.* **1999**, *429* (1−3), 229–236.
(33) Kobayashi, Y.; Akasaka, T. *J. Cryst. Growth* **2008**, *310* (23), 5044–5047.
(34) Reina, A.; Jia, X.; Ho, J.; Nezich, D.; Son, H.; Bulovic, V.; Dresselhaus, M. S.; Kong, J. *Nano Lett.* **2008**, *9* (1), 30–35.
(35) Lin, Y.; Williams, T. V.; Connell, J. W. *J. Phys. Chem. Lett.* **2009**, *1* (1), 277–283.
(36) Nag, A.; Raidongia, K.; Hembram, K. P. S. S.; Datta, R.; Waghmare, U. V.; Rao, C. N. R. *ACS Nano* **2010**, *4* (3), 1539–1544.
(37) Takahashi, T.; Itoh, H.; Takeuchi, A. *J. Cryst. Growth* **1979**, *47* (2), 245–250.
(38) Trehan, R.; Lifshitz, Y.; Rabalais, J. W. *J. Vac. Sci. Technol., A* **1990**, *8* (6), 4026–4032.
(39) Lee, K. S.; Kim, Y. S.; Tosa, M.; Kasahara, A.; Yosihara, K. *Appl. Surf. Sci.* **2001**, *169*, 420–424.
(40) Geick, R.; Perry, C. H.; Rupprecht, G. *Phys. Rev.* **1966**, *146* (2), 543.
(41) Yuzuriha, T. H.; Hess, D. W. *Thin Solid Films* **1986**, *140* (2), 199–207.

DOI: 10.1021/nl1023707 | *Nano Lett.* **2010,** *10,* 4134–4139